Dynamics of the Cyclization Reaction in Photochromic Furyl Fulgides

Martin Handschuh, Martin Seibold, Helmut Port,* and Hans Christoph Wolf

3. Physikalisches Institut, Universität Stuttgart, D-70550 Stuttgart, Germany

Received: June 27, 1996[⊗]

The dynamics of the photoinduced cyclization reaction of furyl fulgides has been studied applying femtosecond time-resolved transient absorption spectroscopy. For furyl fulgide **1** and adamantylidene-substituted furyl fulgide **2** in different solvents, a scheme of the reaction mechanism is set up and the reaction rates are determined by fitting individual transients. Two parallel reaction pathways can be distinguished, one of them including an intermediate state. Reaction times in the picosecond range support the application of fulgides in optical data storage media and as molecular photoswitches.

Introduction

Fulgides are photochromic compounds suitable for use in optical data storage media[1−3] and as molecular functional units such as optical switches.[4] Both fields of application require optical bistability, which is provided by several heteroaromatic fulgides and fulgimides. Irradiation with UV or visible light induces electrocyclic ring-closure/ring-opening reactions, leading to the production of closed **C** or open **E** isomers according to Scheme 1. Generation of the so-called **Z** isomer by UV irradiation of **E** is neglected in the context of this paper, as it can be minimized by proper substitution,[5,6] and does not affect the processes discussed in this paper.

The good photochromic performance of fulgides is based on a combination of the following properties: thermal stability of both isomers at room temperature;[7,8] full reversibility of the photoreactions without photochemical fatigue;[9−11] high conversion efficiencies due to both clearly separated absorption bands with high extinction coefficients[12−14] and high reaction quantum yields;[15,16] and minor environmental effects in liquid solution and rigid polymer matrix.[17,18] Different isomers can be distinguished by means of UV/vis absorption as well as IR spectroscopy, which has been proved to be a totally nondestructive method for detecting the isomerization states.[19]

Although being of crucial importance for the feasibility of optical switches and memories, little is known about the reaction dynamics and the reaction mechanisms of fulgides. Several studies reporting the transient absorption of fulgides after pulse excitation of the respective **E** isomer suffer from insufficient time resolution. Hence, they can only give upper limits for the **E** → **C** reaction times: 20 ps for **1E** in toluene[20] and 10 ps for a furyl fulgide in polymer matrix[21] and 6 ps for a phenyl-substituted fulgide in toluene.[22] As for similar photochromic molecules, 1.1 ps was recently reported for the ring-closure reaction of a diarylethene compound.[23] Following Woodward−Hoffmann's rules,[24] the **E** → **C** isomerization of fulgides is often described as a conrotatory ring-closure reaction. However, experimental data on the relaxation pathway via the ground- and excited-state potential surfaces are missing. Only qualitative models have been proposed for phenyl fulgides[22] and furyl fulgides,[21] implying barrierless relaxation in the excited **E** state.

Here we present transient absorption measurements with femtosecond time resolution of the **E** → **C** isomerization of fulgides **1** and **2** (cf. Scheme 1) which allow us to set up a model for the reaction mechanism and to give quantitative results for the time constants involved.

SCHEME 1: Molecular Structures and Photochromic Reactions E ⇌ C of Fulgides 1 and 2; Absorption Spectra of 2E and 2C in Toluene (295 K)

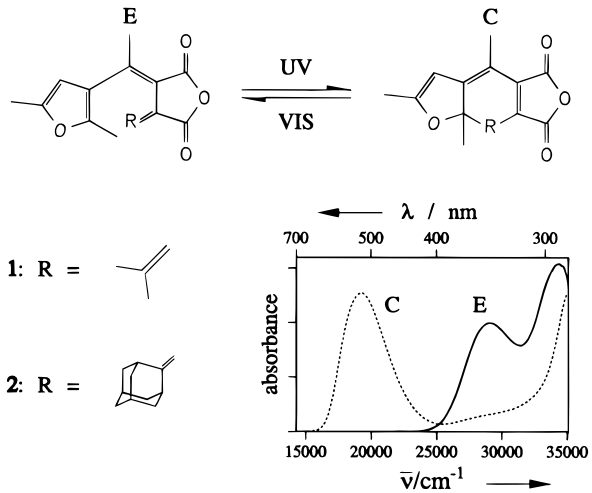

Experimental Section

Time-resolved transient absorption measurements were performed with a pump and probe technique. Pulses are generated using a passively mode-locked Ti:sapphire laser oscillator (Coherent Mira900) pumped by an Ar^{2+} ion laser (Coherent Innova310). A Q-switched, intracavity frequency-doubled Nd:YLF laser (Quantronix 4820) pumps a regenerative Ti:sapphire amplifier (Quantronix 4880) which, after recompression of the previously stretched pulses, supplies 200-fs pulses at 784 nm with a repetition rate of 1 kHz. After splitting this beam in a 20:80 ratio, the lower intensity beam is frequency-doubled in a LBO crystal and used as the pump beam for pulse excitation of the sample at 392 nm (25 500 cm^{-1}; 150 cm^{-1} FWHM; pulse energy 5 μJ). The 80% intensity beam runs through a delay line before being focused on a rotating quartz plate to generate a white light continuum between 10 000 and 24 000 cm^{-1}. The white light is then split into a probe beam, which is focused into the sample such as to achieve maximum overlap with the pump beam, and a reference beam, which is focused into a sample spot not excited by the pump beam. Both transmitted beams are analyzed by a spectrograph and detected by a double-diode array (Hamamatsu S4801-512Q).

The system provides a response time of 300 fs with delay times up to 900 ps. Due to temporal dispersion of the white

[⊗] Abstract published in *Advance ACS Abstracts,* December 15, 1996.

S1089-5639(96)01905-6 CCC: $14.00

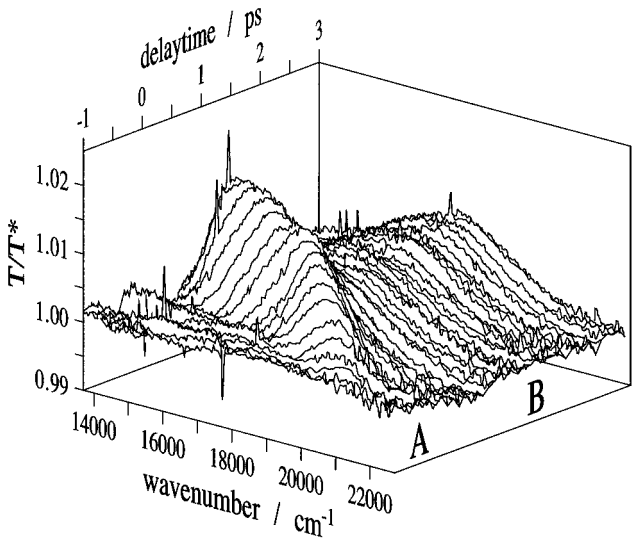

Figure 1. Transient absorption of **2** after pulse excitation of **2E** in acetonitrile ($\bar{\nu}$ = 25 500 cm^{-1}; T = 295 K); ordinate values T/T^*: relative transmission intensities with (T^*) and without (T) excitation. Linear spectral shift of band A with increasing delay time due to temporal white light dispersion of probe pulse (chirp). See text for explanation of bands A and B.

light (chirp), blue spectral components of the probe beam arrive at the sample later than red components, causing the absorption signal at higher energies to appear earlier than at lower energies. Although this effect can numerically be eliminated from the results, we present here uncorrected spectra to give an impression of the original data.

Compounds **1E** and **2E** were purchased from ABERCHROMICS LTD., Cardiff, U.K., and, without further purification, dissolved in toluene or acetonitrile (Merck Uvasol grade). For each pulse, a fresh sample portion was supplied by pumping the solution through a 1-mm flow cell. In order to avoid accumulation of colored **C** isomer in the solution, a 500-mL reservoir was bleached with frequency-doubled Nd:YLF leakage at 527 nm.

For time-resolved fluorescence measurements, a time-correlated single-photon-counting system was used with a frequency-doubled, mode-locked, Nd:YAG laser (Quantronix 416) for pulse excitation at 532 nm; a time resolution of 30 ps was obtained.

Results

Immediately after pulse excitation of **2E** at 25 500 cm^{-1} (392 nm), a strong, rather broad absorption band A rises as shown in Figure 1, where the spectral shift of the signal toward lower wavenumbers, proceeding linearly with delay time, is due to white light dispersion (chirp) of the probe pulse. After fast decay of absorption A within 600 fs, the growth of a narrower band B centered at 17 700 cm^{-1} becomes observable. The intensity of B increases on a 100-ps time scale, while its spectral shape remains unchanged after 1.5 ps (Figure 2). By comparison with the cw absorption of **2C**, band B can be identified as the C_0 ground-state absorption, thus indicating the production of **C** isomer. The qualitative features described here are common for all samples investigated. The rise times of absorption band B are 60 and 70 ps for **1** in acetonitrile and toluene, respectively, and 200 ps for **2** in toluene.

For **2** in toluene, the time evolution of the absorption intensity at 19 200 cm^{-1} can be seen in Figure 3. After an initial increase within the response time of the system, the signal decays with a time constant of 600 fs before slowly increasing after

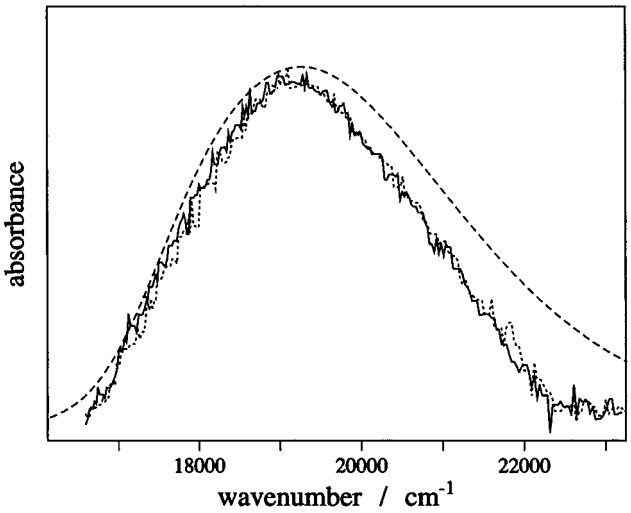

Figure 2. Absorption spectra of **2**, 1.5 ps (—) and 900 ps (- - -) after pulse excitation of **2E** and cw absorption of **2C** (— —), in toluene (295 K).

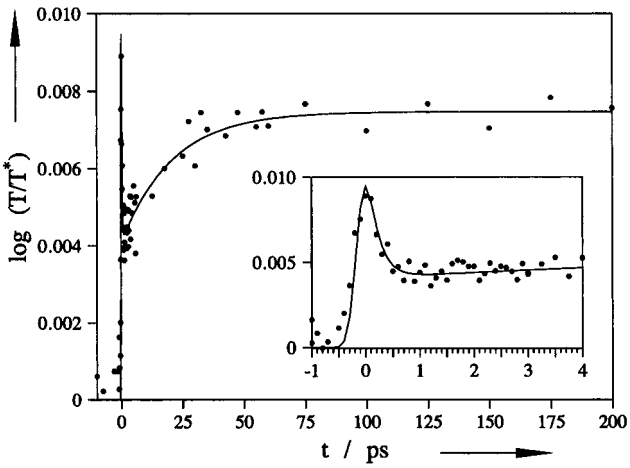

Figure 3. Time evolution of the transient absorption at $\bar{\nu}$ = 19 200 cm^{-1} after pulse excitation of **2E** in toluene (295 K): experimental data (●) and fitted model curve (—); notice stretched abscissa in insert.

approximately 1 ps and approaching a constant maximum value at 200 ps. According to Figure 1, the first intensity peak can be attributed to absorption band A, whereas for long delay times the absorption signal is due to band B. Taking the minimum intensity at 1 ps as 100%, the overall signal recovery is 100% for **2** in toluene; for **1** in acetonitrile and toluene, the corresponding values are 30% and 40%. At very long delay times of several hundred picoseconds, a slight decrease of absorption intensity was observed for **1** and **2** in toluene; however, since we did not find uniform behavior and the effect was not significant at given signal-to-noise ratio, it is not considered in the interpretation of the experimental results.

Model Description

In order to carry out a quantitative analysis of the experimental results, a model for the mechanism of an optically induced reaction **E** → **C** between two thermally stable isomers is set up (Figure 4). Since the model is defined as the general excited state diagram, no assumptions on the specific reaction mechanism are implied. In particular, only as many states are included as are necessary to describe the time evolution of the absorption signal as shown in Figure 3. Thus, it is sufficient to consider the ground and excited states E_0 and E* of the **E** isomer and C_0 and C* of the **C** isomer as well as an intermediate

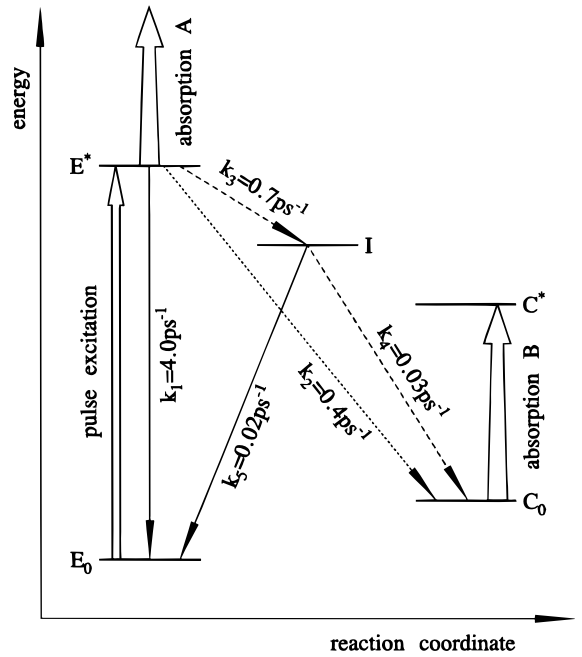

Figure 4. Model diagram for the **E** → **C** reaction mechanism of furyl fulgides **1** and **2**.

state I on the reaction pathway E* → C_0 whose nature needs not to be specified; nevertheless, I is indispensable for explaining why the rise time of B differs from the decay time of A.

All possible transitions between participating states are taken into account. Starting from E_0, pulse excitation creates population of E* which relaxes radiatively and/or nonradiatively to the ground state E_0 (rate constant k_1); alternatively, transitions from E* to C_0 with rate constant k_2 and to I with k_3 take place. From I relaxation both to C_0 (k_4) and to E_0 (k_5) is possible. Because of the thermal stability of the **E** and **C** isomers, no transistions between the E_0 and C_0 ground states are considered. While stimulated emission is neglected, all states involved can, in principle, contribute to the white light absorption of the probe pulse.

With the model set up according to Figure 4, the reaction kinetics can completely be described by a set of differential equations for the time derivatives of the populations $N_{E^*}(t)$, $N_I(t)$, and $N_{C_0}(t)$ of states E*, I, and C_0 at time t after excitation:

$$\dot{N}_{E^*}(t) = -(k_1 + k_2 + k_3)N_{E^*}(t) \quad (1)$$

$$\dot{N}_I(t) = k_3 N_{E^*}(t) - (k_4 + k_5)N_I(t) \quad (2)$$

$$\dot{N}_{C_0}(t) = k_2 N_{E^*}(t) + k_4 N_I(t) \quad (3)$$

(1) directly yields

$$N_{E^*}(t) = N_0 e^{-kt} \quad (4)$$

with $N_0 \equiv N_{E^*}(0)$ being the initial population of E* after pulse excitation and

$$k \equiv k_1 + k_2 + k_3 \quad (5)$$

If we further define

$$\bar{k} \equiv k_4 + k_5 \quad (6)$$

and consider the boundary conditions $N_I(\infty) \stackrel{!}{=} 0$ and $N_I(0) \stackrel{!}{=} 0$, we obtain

$$N_I(t) = N_0 \frac{k_3}{k - \bar{k}}(e^{-\bar{k}t} - e^{-kt}) \quad (7)$$

and

$$N_{C_0}(t) = N_0\left\{\frac{k_2}{k}(1 - e^{-kt}) + \frac{k_3 k_4}{k - \bar{k}}\left[-\frac{1}{k}(1 - e^{-kt}) + \frac{1}{\bar{k}}(1 - e^{-\bar{k}t})\right]\right\} \quad (8)$$

It follows from (8) and $N_{C_0}(\infty) \stackrel{!}{=} \phi_{EC} N_0$, with ϕ_{EC} being the **E** → **C** reaction quantum yield, that

$$\phi_{EC} = \frac{k_2\bar{k} + k_3 k_4}{k\bar{k}} \quad (9)$$

If only states E*, I, and C_0 contribute to the white light absorption, the optical density OD of a sample at wavenumber $\bar{\nu}$ at time t is given by

$$OD_{\bar{\nu}}(t) = \alpha[N_{E^*}(t)\epsilon_{E^*,\bar{\nu}} + N_I(t)\epsilon_{I,\bar{\nu}} + N_{C_0}(t)\epsilon_{C_0,\bar{\nu}}] \quad (10)$$

where α is a factor representing thickness and molar concentration of the sample and $\epsilon_{S,\bar{\nu}}$ are the molar extinction coefficients of states S at wavenumber $\bar{\nu}$. If we set $\phi_{CE} = k_5/\bar{k}$ and define

$$\epsilon_1 \equiv \frac{\epsilon_{E^*,\bar{\nu}}}{\epsilon_{C_0,\bar{\nu}}} \qquad \epsilon_2 \equiv \frac{\epsilon_{I,\bar{\nu}}}{\epsilon_{C_0,\bar{\nu}}} \quad (11)$$

inserting (4), (7), (8), and (9) in (10) yields

$$OD_{\bar{\nu}}(t) = \alpha_{\bar{\nu}}\left[\left(\epsilon_1 - \epsilon_2\frac{k_3}{k - \bar{k}} + \frac{k_3(1 - \phi_{CE})}{k - \bar{k}} - \phi_{EC}\right)e^{-kt} + (\epsilon_2 + \phi_{CE} - 1)\frac{k_3}{k - \bar{k}}e^{-\bar{k}t} + \phi_{EC}\right] \quad (12)$$

(12) serves as model expression for the transient absorption of the sample after pulse excitation at $t = 0$. After convolution with the system response function of the setup, the model function can numerically be fitted to the experimental data, i.e., the temporal evolution of the transient absorption at a certain wavenumber $\bar{\nu}$, thus providing a set of parameters $\{\alpha_{\bar{\nu}}, k, \bar{k}, k_3, \epsilon_{1,\bar{\nu}}, \epsilon_{2,\bar{\nu}}\}$ from which k_i and $\epsilon_{S,\bar{\nu}}$ can be obtained.

Discussion

Identification of the absorption signals observed in Figure 1 is facilitated by the lack of E* ← E_0 absorption in the visible range. Because of its quasi-instantaneous appearance, absorption band A must be attributed to the transient absorption of the **E** isomer, i.e., an excitation from E* to higher excited states by the white light probe pulse. Upon closer inspection, band A turns out to be a superposition of a slowly increasing contribution of band B as well as two separate absorption bands centered at 15 000 and 19 000 cm^{-1} and with slightly different rise times. The nature of these absorptions can not yet be explained satisfactorily; however, vibrational relaxation in the E* state seems to play a role. Changing the solvent polarity μ affects the shape of band A; for both **1** and **2** in polar acetonitrile ($\mu = 3.4$ D), the contributions of the absorptions at 15 000 and 19 000 cm^{-1} are about equal, leading to the plateaulike shape of A, whereas in less polar toluene ($\mu = 0.35$ D), the absorption at higher wavenumber is significantly stronger, causing the shape of A to become asymmetric. Hence, the excited-state geometry of **E** is assumed to be polar.

No significant absorption of the intermediate state I can be found. Absorption band B can be identified as the C_0 ground-

TABLE 1: Model Parameters Obtained for Reaction Rates k_i (ps^{-1}), Time Constants τ_i (ps), and Relative Extinction Coefficients $\epsilon_{j,\bar{\nu}}$ of 1 and 2 in Toluene (tol) and Acetonitrile (acn) at Maxima of Band B[a]

		$\bar{\nu}$, cm^{-1}	k_1	k_2	k_3	k_4	k_5	τ_1	τ_2	τ_3	τ_4	τ_5	$\epsilon_{1,\bar{\nu}}$	$\epsilon_{2,\bar{\nu}}$
1	tol	19 600	2.9	0.3	0.4	0.1	0.004	0.3	3.3	2.7	16	230	0.3	≈0
	acn	18 800	3.7	0.4	0.4	0.1	0.004	0.3	2.8	2.3	12	250	0.3	≈0
2	tol	19 200	4.0	0.4	0.7	0.1	0.02	0.3	2.6	1.4	32	62	0.4	≈0
	acn	17 700												

[a] As the measurements on **2** in acetonitrile were limited to short delay times, numerical analysis was not possible.

state absorption of the closed **C** isomer since the center wavenumber and spectral shape agree with those of the cw absorption of **C** (cf. Figure 2). As C_0 is the final state of the reaction process, the appearance of band B indicates the photoreaction **E** → **C** of a certain number of molecules; in particular, when B reaches its maximum intensity, the conversion of a fraction ϕ_{EC} of the excited molecules is complete.

The convolution of model function (12) with the Gaussian system response function can be fitted to the experimental data, i.e., the time evolution of the transient absorption at a certain wavenumber $\bar{\nu}$, as exemplified in Figure 3; this procedure yields a set of reaction rates k_i, corresponding time constants $\tau_i = 1/k_i$, and relative molar extinction coefficients $\epsilon_{j,\bar{\nu}}$ (cf. eq 11), with an uncertainty of ±30% inherent to the numerical analysis. Table 1 summarizes the results obtained by this method for **1** and **2** in toluene and acetonitrile. Reaction quantum yields are ϕ_{EC} = 18% and ϕ_{CE} = 8.4% for **1** in toluene, ϕ_{EC} = 17% and ϕ_{CE} = 4.8% for **1** in acetonitrile, and ϕ_{EC} = 17% and ϕ_{CE} = 34% for **2** in toluene.

No E* fluorescence could be detected; thus, since k_1 is larger than k_2 and k_3 by 1 order of magnitude, the fast decay of the E* transient absorption (band A) is caused by nonradiative relaxation E* → E_0. Transitions from E* to I and C_0 are of the same order of magnitude. I decays much more slowly than E*; in the case of **1**, relaxation from I is mainly to C_0 as reflected by the respective k_4/k_5 ratios. Independent of solvent, substitution, and wavenumber, we find the general relation $\epsilon_{1,\bar{\nu}} \gg \epsilon_{2,\bar{\nu}} \approx 0$ within the error limits of the numerical analysis. We therefore do not consider the transient absorption of state I in the interpretation of the absorption spectra obtained from our time-resolved measurements (e.g. Figure 1).

For **1**, the relaxation from I to C_0 is faster than for **2**, as indicated by rate constants k_4 and relaxation times τ_4. This is in agreement with the observation of shorter rise times (60, 70 ps) of absorption band B for **1** as compared to **2** (200 ps). On the cyclization reaction coordinate, I might be shifted toward the **E** isomer by substitution of a bulky adamantylidene group, thus reducing the I → C_0 transition rate.

Reaction Pathways. After excitation of **E**, the ring-closure reaction **E** → **C** proceeds via two different pathways: firstly, on a fast direct pathway P_1, E* → C_0; secondly, on a slow indirect pathway P_2, E* → I → C_0. The relative weight of P_1 and P_2 is given by the ratio $P_1/P_2 = k_2/(k_3[k_4/(k_4 + k_5)])$. For compound **1**, both pathways are about equally important: $P_1/P_2 \approx 0.9$; i.e., 53% of the molecules undergoing ring closure use the indirect pathway P_2. On the other hand, for **2** in toluene, investigation yields $P_1/P_2 \approx 0.8$; therefore, the contribution of P_2 is somewhat larger, namely 56%.

In both cases, the intermediate state I works as a bottleneck, delaying the transition from E* to C_0 on account of its rather long lifetime ($\tau_4 > 10$ ps) as compared to E* ($\tau_1 \leq 0.3$ ps). As a consequence, the absorption band B does not increase monoexponentially; after fast buildup of about 50% via P_1 with $\tau_2 \approx 3$ ps, the absorption approaches its maximum intensity via P_2 on a 100-ps time scale. We have no evidence for the nature of I nor for its energetic position relative to C*; it seems to be very unlikely that I is an excited **C** state C* because upon excitation of **E**, no fluorescence of **C** can be detected. In addition, the time constant of the fluorescence decay of **2C** upon excitation at 18 800 cm^{-1} is larger than 100 ps and therefore much larger than the time constant for the relaxation of I.

Switching Times. The photoisomerization **E** ⇌ **C** of fulgides can be used for optical data storage and imaging; it can also be regarded as a reversible optically induced switching process. For the photoinduced cyclization **E** → **C** examined, two "switching times" can be defined on the basis of our time-resolved measurements:

(1) The first switching time is the time delay between the excitation and the detection of C_0 population; this is determined by time constants τ_1 and τ_2 and corresponds to the closing of a photoswitch or to the minimum write → read delay in a recording device.

(2) The second switching time is the time delay between the excitation and the completion of the photoreaction, i.e., maximum population of C_0 without measurable change; this is governed by the largest of the time constants τ_3, τ_4, and τ_5 and corresponds to the minimum write → erase delay in a recording device.

The existence of C_0 population according to case 1 is indicated by the observation of C* ← C_0 absorption and thus by band B. Following the definition given above, our experiments yield switching times of approximately 1 ps for **1** and **2**, depending mainly on the time constants of the direct reaction pathway P_1.

The photoreaction is completed in the sense of definition 2 when band B reaches its maximum intensity. Thus, the corresponding switching times are 70 (60) ps for **1** in toluene (acetonitrile) and 200 ps for **2** in toluene. They are determined by the time constants of the indirect reaction pathway P_2.

Conclusions

The transient absorption of two furyl fulgides was investigated with a subpicosecond time resolution. Based on the temporal evolution of the absorption spectra, a model for the mechanism of the cyclization reaction can be set up; this includes the ground and excited states of **E** and **C** isomers as well as an intermediate state whose nature is not evident. According to our model, cyclization proceeds via two distinct pathways: a direct pathway from the E* excited state to the C_0 ground state and an indirect pathway via the intermediate state I. The time demand of the photocyclization depends on the process considered: while for optical switching or recording of data the time constant is approximately 1 ps, it is on a 100-ps time scale for the less time-critical write → erase cycle in an optical storage device.

Acknowledgment. Support from the Deutsche Forschungsgemeinschaft (SFB 329) and Fonds der Chemischen Industrie is gratefully acknowledged.

References and Notes

(1) Hirshberg, Y. *J. Am. Chem. Soc.* **1956**, *78*, 2304.
(2) Psaltis, D. *Byte* **1992**, *17*, 179.
(3) Matsui, F.; Taniguchi, H.; Yokoyama, Y.; Sugiyama, K.; Kurita, Y. *Chem. Lett.* **1994**, 1869.
(4) Walz, J.; Ulrich, K.; Port, H.; Wolf, H. C.; Wonner, J.; Effenberger, F. *Chem. Phys. Lett.* **1993**, *213*, 321.
(5) Ulrich, K.; Port, H.; Wolf, H. C.; Wonner, J.; Effenberger, F.; Ilge, H.-D. *Chem. Phys.* **1991**, *154*, 311.
(6) Kiji, J.; Okano, T.; Kitamura, H.; Yokoyama, Y.; Kubota, S.; Kurita, Y. *Bull. Chem. Soc. Jpn.* **1995**, *68*, 616.

(7) Heller, H. G. In *Electronic Materials. From Silicon to Organics*; Miller, L. S., Mullin, J. B., Eds.; Plenum: New York, 1991; p 471.

(8) Suzuki, H.; Tomoda, A.; Ishizuka, M.; Kaneko, A.; Furui, M.; Matsushima, R. *Bull. Chem. Soc. Jpn.* **1989**, *62*, 3968.

(9) Heller, H. G. *Spec. Publ.—R. Soc. Chem.* **1986**, *60* (Fine Chemicals for the Electronic Industry), 120.

(10) Kaneko, A.; Tomoda, A.; Ishizuka, M.; Suzuki, H.; Matsushima, R. *Bull. Chem. Soc. Jpn.* **1988**, *61*, 3569.

(11) Ulrich, K.; Port, H. *J. Mol. Struct.* **1990**, *218*, 45.

(12) Tomoda, A.; Kaneko, A.; Tsuboi, H.; Matsushima, R. *Bull. Chem. Soc. Jpn.* **1992**, *65*, 1262.

(13) Heller, H. G.; Hughes, D. S.; Hursthouse, M. B.; Koh, K. V. S. *J. Chem. Soc., Chem. Commun.* **1994**, 2713.

(14) Sun, Z.; Hosmane, R. S.; Tadros, M. *Tetrahedron Lett.* **1995**, *36*, 3453.

(15) Glaze, A. P.; Heller, H. G.; Whittall, J. *J. Chem. Soc., Perkin Trans.* **1992**, *2*, 591.

(16) Yokoyama, Y.; Inoue, T.; Yokoyama, M.; Goto, T.; Iwai, T.; Kera, N.; Hitomi, I.; Kurita, Y. *Bull. Chem. Soc. Jpn.* **1994**, *67*, 3297.

(17) Yokoyama, Y.; Hayata, H.; Ito, H.; Kurita, Y. *Bull. Chem. Soc. Jpn.* **1990**, *63*, 1607.

(18) Seibold, M.; Port, H.; Wolf, H. C. *Mol. Cryst. Liq. Cryst.*, in press.

(19) Seibold, M.; Port, H. *Chem. Phys. Lett.* **1996**, *252*, 135.

(20) Parthenopoulos, D. A.; Rentzepis, P. M. *J. Mol. Struct.* **1990**, *224*, 297.

(21) Kurita, S.; Kashiwagi, A.; Kurita, Y.; Miyasaka, H.; Mataga, N. *Chem. Phys. Lett.* **1990**, *171*, 553.

(22) Ilge, H.-D.; Sühnel, J.; Khechinashvili, D.; Kaschke, M. *J. Photochem.* **1987**, *38*, 189.

(23) Tamai, N.; Saika, T.; Shimidzu, T.; Irie, M. *J. Phys. Chem.* **1996**, *100*, 4689.

(24) Woodward, R. B.; Hoffmann, R. *J. Am. Chem. Soc.* **1965**, *87*, 395, 2046, 2511.